Thin Solid Films 727 (2021) 138676

Contents lists available at ScienceDirect

Thin Solid Films

journal homepage: www.elsevier.com/locate/tsf

Influence of post-deposition annealing on the transport properties of sputtered Bi_2Se_3 thin films

Yub Raj Sapkota, Dipanjan Mazumdar *

Physics Department, Southern Illinois University, Carbondale, IL, 62901, USA

ARTICLE INFO

Keywords:
Topological Insulators
Thin films
Magnetron Sputtering
Spintronics

ABSTRACT

The fabrication of chalcogenide-based topological insulator (TI) thin films with low defects and vacancies is an important research problem. In the past decade, Bi_2Se_3 is one of the most investigated TI materials. The physical properties of Bi_2Se_3 are dictated by selenium vacancies irrespective of the growth method. Controlling the number of vacancies is very challenging, but it can be influenced by substrate and growth temperature. In this work, we demonstrate that post-deposition annealing temperature is also effective in controlling the carrier concentration of Bi_2Se_3 thin films. Ultra-thin Bi_2Se_3 films were fabricated on quartz substrates using magnetron sputtering at room temperature, and their resistivity, bulk carrier concentration, and bulk mobility are measured as a function of the post-deposition annealing temperature under vacuum conditions ranging from 180–350 °C. We find that the carrier concentration can vary by an order of magnitude, and we obtained values as low as $\sim 1 \times 10^{19}$ cm^{-3} between 200-250 °C which compares very well with some of the best literature reports on films made by molecular beam epitaxy. Room temperature bulk mobility values in excess of 100 cm^2/Vs were recorded for the optimally annealed samples. Energy dispersive x-ray spectroscopy measurements showed that selenium-rich Bi_2Se_3 films have the highest carrier concentration values. X-ray diffraction measurements showed that the best crystallographic properties are obtained for stoichiometric Bi_2Se_3. Our results indicate that higher mobility values may be possible if better crystal structure and lower resistivity are obtained in selenium-rich films.

1. Introduction

The discovery of a number of Bismuth-based 3D topological insulators (TI) at room temperature [1–5] has generated significant interest in areas such as spintronics [6–10], semiconductors [11], plasmonics [12,13], Terahertz photodetection [14,15] and fault-tolerant quantum computing [16–18]. The most promising TI materials are low band gap chalcogenides such as Bi_2Se_3 and Bi_2Te_3. Despite the confirmation of the protected surface-states through photoemission measurements [4,3,5], device applications rely on electronically isolating the surface states from the overwhelmingly large concentration of bulk carriers. Therefore, there is significant interest to grow high quality TI thin-films using methods such as molecular beam epitaxy (MBE) [19–27], chemical vapour depositon (CVD) [28,29], plused laser deposition (PLD) [30–34], and magnetron sputtering [35–37].

In an MBE process, the individual elements are co-evaporated in an ultra-high vacuum environment. This leads to a highly controlled and epitaxial growth of TI thin films [38–41]. Compared to MBE, PLD and magnetron sputtering are more aggressive and typically employ a process gas such as Argon to fabricate TI thin films [30]. However, it can be argued that both MBE and PLD may be too expensive for device applications when compared to CVD and magnetron sputtering [41,42]. CVD is not a preferred method for growing heterostructures since it may lead to contamination during the sample transfer process [41]. Growth of TI thin films using magnetron sputtering is receiving significant attention, particularly for spintronics applications. Recent research on Bi_2Se_3-CoFeB bilayers, grown entirely using magnetron sputtering, demonstrated higher spin-orbit torque on the ferromagnetic CoFeB layer compared to MBE-grown Bi_2Se_3 [7]. Such studies highlight that magnetron sputtering may be more suitable for certain applications.

Transport properties of chalcogenide-based TI materials such as Bi_2Se_3 are dominated by unintentional *n*-type doping due to the presence of native defects such as chalcogen (Se) vacancies or antisites [43], irrespective of the growth conditions (e.g., Bi-rich or Se-rich) [44] or method (single crystal, thin films) [45,34]. Selenium vacancies have been mapped using scanning tunneling microscopy in Bi_2Se_3 films [46] and cleaved crystals [44]. In thin films, carrier concentrations are

* Corresponding author: Southern Illinois University Carbondale, Physics Department, 1245 Lincoln Drive, Carbondale, IL, 62901, USA.
E-mail address: dmazumdar@siu.edu (D. Mazumdar).

https://doi.org/10.1016/j.tsf.2021.138676
Received 7 July 2020; Received in revised form 18 March 2021; Accepted 1 April 2021
Available online 5 April 2021
0040-6090/© 2021 Elsevier B.V. All rights reserved.

typically in the $\sim 10^{19}$-10^{20} cm^{-3} range and values below 10^{18} cm^{-3} are difficult to obtain. The lowest bulk carrier concentration ($\sim 10^{16}$ - 10^{17} cm^{-3}) are reported on single crystals [45,47]. A theoretical study has indicated that a carrier concentration of 1×10^{15} cm^{-3} may be possible [43].

Tranport properties of thin films are also controlled by the film-substrate interface. Typically, the resistivity (mobility) increases (decreases) significantly at the ultra thin-film level due to higher scattering at the film-substrate interface [34,48]. Several studies also show that carrier concentration also varies significantly at the ultra-thin film level [48,49]. The best quality 5–10 nm Bi_2Se_3 thin films grown on standard substrates (Al_2O_3, Si/SiO_2, Si) show carrier concentration values in the (0.5-2) $\times$ 10^{19} cm^{-3} range [8,19,22,32,50–52]. Koirala *et al.* [49] demonstrated that carrier concentration can be reduced by up to an order of magnitude by employing suitable substrate and interface engineering that also resulted in ultra-high surface mobility of up to 16000 cm^2/Vs at 2 K. Such values already approach the best single crystal results [47]. Other strategies to lower carrier cocencentration values involve substitutional doping of Bi with Sb [53] .

Reports on Bi_2Se_3 films grown with magnetron sputtering are relatively sparse. Some studies on magnetron sputtered Bi_2Se_3 films highlighted the role of substrate temperature on the Bi:Se ratio [37,36,54, 55]. While high temperature is generally preferred for epitaxial growth, it typically results in high concentration of selenium vacancies [36,37]. Therefore, some groups combined room or high temperature growth with subsequent Selenium annealing [55,56]. In our previous work, we established and characterized the optical [57] and transport [58] properties of 2-100 QL Bi_2Se_3 grown at room temperature and annealed under high vacuum for 2 h at 300 °C. The conditions were optimized to promote the highest x-ray diffraction intensity and reaffirmed in this work. Despite high crystalline quality, transport measurements [*58*] indicated that the properties were significantly inferior compared to MBE grown films as evidenced through high carrier concentration ($\sim 10^{20}$ cm^{-3}) and a low Hall mobility of ~ 25 cm^2/V.s for a 6 QL sample grown on amorphous quartz. This provided the motivation to correlate the growth-structure-property relationships in greater detail and test the limits of the sputtering process.

In this work, we show that the transport properties can be substantially improved by adjusting the post-deposition vacuum annealing conditions. We observed low carrier concentration ($\sim 1 \times 10^{19}$ cm^{-3}) and significantly higher mobility values (112 cm^2/V.s) in ultra-thin samples annealed between 220-250 °C for 30 min. This improvement is significant compared to our previous work [58] and compares very well with the best values reported using MBE. Low carrier concentration and high mobility values are observed in selenium rich samples, whereas the best crystal quality is observed in stoichiometric (Bi:Se = 2:3) samples when annealed at 300 °C. Overall, we show that our sputter deposition method can produce high quality TI thin films with superior transport properties and infer that the method can be extended to other TI materials.

2. Experimental details

Ultrathin Bi_2Se_3 thin films of nominal 7 nm thickness were rf sputtered onto 10 $\times$ 10 mm^2 amorphous quartz substrate from a stoichiometric target (Kurt Lesker, 99.999% purity) at 6.66 Pa Ar gas pressure in a high vacuum chamber (base pressure 5.3 $\times$ 10^{-7} Pa). Samples were sputtered at room temperature and subsequently annealed *in-situ* for 30 min at various temperatures between 180-350 °C. Thickness, roughness, and density of films were obtained using the X-ray reflectivity (XRR) method and crystal structure was determined by employing the X-ray diffraction (XRD) method. Both XRR and XRD measurements were performed using a Rikagu Smartlab Diffractometer with Cu-Kα radiation. The elemental composition was examined using energy dispersive X-ray (EDX) spectroscopy at an accelerating 20 kV beam spot of 3-3.5 mm equipped with FEI Quanta EFG 450SEM. Longitudinal resistivity (ρ) and Hall measurements were performed at 0.7 Tesla using a NanoMagnetics Instruments ezHEMS system in the Van-der-Pauw (VDP) geometry to extract the bulk carrier concentration ($n_{3D} = 1/(eR_H)$, where R_H is the Hall coefficient and e is the elementary charge), and Hall mobility ($\mu = R_H/\rho$). The surface carrier concentration is extracted from the bulk concentration, $n_{2D} = n_{3D}t$, where t is the thickness of film. The four-probe contact was made using Au/Cr tips on silver paint placed at the corners of square samples. This provided a linear Current-Voltage curve.

3. Results and discussions

In Fig. 1a, we show the representative XRR data of a $\sim$7 nm Bi_2Se_3 thin film annealed at 180 °C. Pronounced oscillations patterns are revealed with sharp interfaces, and a surface roughness value of less than 0.5 nm was obtained after data fitting. Ultra-smooth and uniform samples were obtained under other annealing conditions. Also, we fitted the X-ray reflectivity data with an oxide layer and did not find any noticeable improvement to the fit. This finding is similar to our earlier conclusion from optical spectroscopy [57]. Taking all the data into consideration, the surface oxidation effect will be neglected throughout the rest of our discussion.

In Fig. 1b, we show the XRD pattern of all films annealed between 180–350 °C. No XRD pattern was observed for the room-temperature sample indicating that the as-grown films are amorphous in nature. Measureable XRD intensity is observed when annlead above 150 °C. The XRD patterns only show (00*3*) family of peaks which confirms that all films are highly textured and oriented along the trigonal axis which is associated with Bi_2Se_3. We plot the intensity of the (00*6*) diffraction peak in the inset figure to highlight the annealing temperature dependence. As observed, the intensity increased by a factor of 4 as the temperature is increased from 180-300 °C. The intensity is a maximum at 300 °C and fell sharply at 350 °C. The reduced intensity at 350 °C is due to a combination of polycrystalline growth and higher defects and vacancies. Prolonged annealing at 350 °C (about 2 h) led to chemical decomposition to Selenium deficient phases (data not shown). We thereby conclude that the best crystal structure is obtained when samples are annealed at 300 °C, which is consistent with our previous report [58]. The annealing time is significantly reduced in this work (30 mins vs 2 h in Ref. [58]). As we show, reducing the annealing time significantly improved the transport properties.

EDX measurements revealed that the composition of the films vary strongly with annealing temperature, as summarized in Table 1. We find that films annealed at 180 °C are significantly selenium rich (Bi:Se = 1:3) even though our target composition is stoichiometric (2:3). Annealing at higher temperatures reduced the relative selenium content, and the composition is very close to 2:3 at 300 °C. The selenium-rich nature at lower annealing temperatures (180-250 °C) – and presumably in as-deposited samples - – implies that the sputtering process removes Selenium from the Bi_2Se_3 target at a much higher rate than Bismuth. This could be due to the low binding energy of Selenium. Therefore, post-deposition annealing, in effect, is serving two purposes. One is to promote better crystallinity, and the other is to control the selenium content. While the creation of selenium vacancies was expected with annealing, the formation of selenium rich films during deposition was unexpected . It is to be noted that the best crystal quality from XRD measurements (Fig. 1b) corresponded to the stoichiometric 2:3 ratio. Additional evidence to support that the sputtering process removes Selenium at a disproportionately high rate from the target was confirmed through a direct XRD scan of the nominal Bi_2Se_3 target after prolonged usage. As shown in Fig. 2, the surface of the used sputtering target matched the XRD pattern of BiSe instead of Bi_2Se_3 which points to high selenium deficiency. XRD profile matching Bi_2Se_3 composition was recovered after polishing the used target (data not shown). Put together, we conclude that the sputtering process resulted in a transfer of selenium-rich Bismith selenide thin films. This observation has

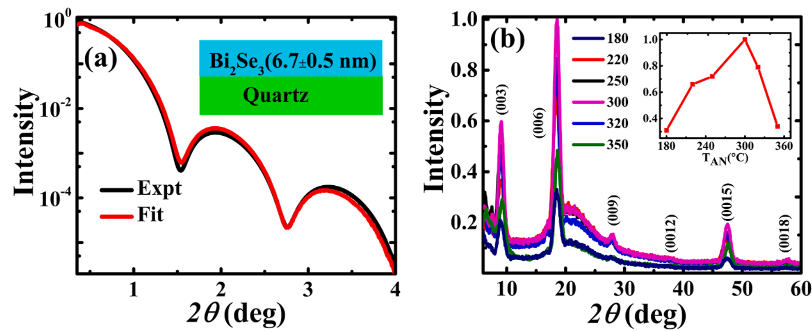

Fig. 1. (a) X-ray reflectivity data of a Bi_2Se_3 sample grown on quartz substrate and annealed at 180 °C. The extracted thickness and roughness is shown in the inset. (b) Variation of X-ray diffraction pattern with annealing temperature as indicated. Inset of (b) shows variation of the (006) XRD peak with annealing temperature. Highest intensity is observed at 300 °C.

Table 1
Elemental ratio of Bismuth and Selenium vs post-deposition annealing temperature measured using Energy Dispersive X-ray spectroscopy. The carrier concentration values obtained from Hall measurements are also tabulated.

Annealing Temp. (° C)	Bismuth (Atomic %)	Selenium (Atomic %)	n_{3D} (cm^{-3})	n_{2D} (cm^{-2})
180	25	75	1.40×10^{19}	1.04×10^{13}
220	35	64	1.34×10^{19}	1.07×10^{13}
250	37	63	2.29×10^{19}	1.60×10^{13}
300	40	60	3.95×10^{19}	2.77×10^{13}
350	45	55	1.09×10^{20}	8.73×10^{13}

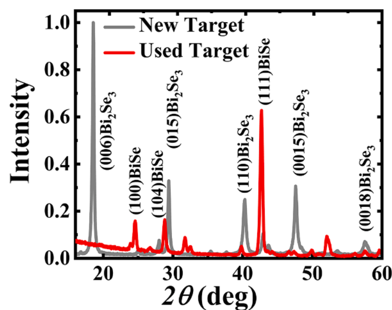

Fig. 2. Surface XRD pattern of the new (gray) and the used (red) Bismuth selenide sputtering target employed during this work. The diffraction pattern of the used target is very close to BiSe (1:1) composition, whereas the new target is Bi_2Se_3 (2:3). The disproportionate removal of Selenium from the target results in Selenium-rich films.

interesting implications on the transport properties as we discuss next.

We observe that Bi:Se ratio has a strong influence on the carrier concetration as shown in Table I and plotted in Fig. 3. Selenium rich samples showed much lower carrier concentration. In particular, samples annealed at 180 and 220 °C show values very close to 1×10^{19} cm^{-3}. These values compare very well to some of the best MBE and PLD grown samples [34,40]. Above 220 °C, the concentration increased very slowly and is 4×10^{19} cm^{-3} at 300 °C. Above 300 °C, the carrier concentration is seen to increase very rapidly and is over 10^{20} cm^{-3} by 350 °C, which is similar to the values reported by other groups [35–37]. It is to be noted that the melting point of selenium (220 °C) coincides very well with the onset of the increase in the carrier concentration values. However, as noted previously, low annealing temperatures do not correspond to the best crystal structure - which is observed at 300 °C

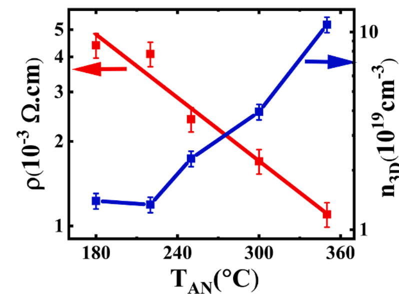

Fig. 3. Variation of room temperature resistivity (ρ) and bulk carrier concentration (n_{3D}) for samples treated with different post-deposition annealing temperature (T_{AN}) as indicated.

(Fig. 1b). So we conclude that the conditions for the lowest carrier concentration and the best crystal structure do not coincide.

The bulk resistivity, on the other hand, decreased practically linearly throughout, as shown in Fig. 3, with values ranging between 4.4 mΩ.cm at 180 °C to 1.1 mΩ.cm at 350 °C. *N*-type behavior is observed in all films which is attributed to selenium vacancies. While resisitivity can also decrease due to improved crystal structure, we infer that the decrease is primarily due to the increase in carrier concentration.

We have summarized all major transport data in Table 2 including the bulk resistivity (ρ), the Hall coefficient (R_H), and the Hall mobility (μ). We can see that the Hall coefficient has a clear maximum at 220 °C and decreased almost in the same proportion as the resisitivity as the annealing temperature is increased from 220 °C to 250 °C. As a result, the Hall mobility is fairly constant in the 220-250 °C range, with values close to 110 cm^2/V.s, as shown in Fig. 4a. The mobility and resistivity variation with sample temperature are plotted in Fig. 4b for the sample annealed at 250 °C. The monotonous decrease in resistivity down to 87 K indicates metallic behavior [59]. We observed higher resistivity values than our previous report [58] which we attribute to lower carrier concentrations in our present work. The resistivity values shown in Fig. 4b (2.8 mΩ.cm at room temperature and 2.67 mΩ.cm at 95 K) are comparable to values reported on MBE and PLD films [9,34]. Unlike our

Table 2
Variation of Bulk Resistivity (ρ), Hall coefficient (R_H), and mobility (μ) with annealing temperature (T_{AN}). All samples show *n*-type behavior and measurements are performed at room temperature.

T_{AN} (°C)	ρ (Ω.cm)	R_H ($Ω.cm^3$/ V.s)	μ (cm^2/V.s)
180	0.0044	0.416	91.55± 4.82
220	0.0041	0.465	111.80 ± 5.92
250	0.0024	0.271	109.61 ± 3.77
300	0.0017	0.157	88.94 ± 5.78
350	0.0011	0.057	50.55 ± 2.69

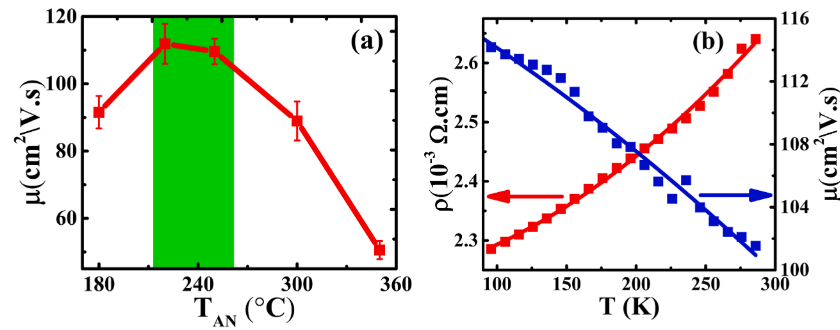

Fig. 4. (a) Variation of mobility as a function of the post-deposition annealing temperature. The shaded region highlights the temperature range with the highest mobility values. (b) Temperature dependence of resistivity and mobility for the sample annealed at 250 °C.

previous result [58], where we observed a strong linear behavior, the present temperature dependence shows a weak non-linear behavior. Similarly, the mobility increased by a modest amount from 101 cm^2/V.s at room temperature to 115 cm^2/V.s at 95 K. This increase is controlled by the resistivity variation as the Hall coefficient, R_H, does not show any specific trend (data not shown).

A few comments are necessary to clarify what may appear as contradictory. First, it may seem conflicting that nominally Se-rich samples - as inferred from EDX data - also show Se vacancies as indicated by the metallic transport behavior. We attribute this to the formation of local Se vacancies in an overall Se-rich sample. Our data is consistent with Analytis *et al.* [45] who report metallic behavior on Se-rich, single--crystal Bi_2Se_3 with low carrier concentration (~3 × 10^{17} cm^{-3}). Urazhdin *et al.* [44] showed that both Bi and Se-rich samples behave as n-type materials. Our data implies that local vacancies are significant above 180 °C, but samples remain overall Se-rich to up to 300 °C. We can only speculate at this point as to where the excess Selenium atoms are located as Bi_2Se_3 starts to crystallize. Xue *et al.* pointed out that Se antisite defects are more stable in Bi-poor/Se-rich samples [43]. It is also likely that the excess Se occupy interstitial sites.

Our data might also appear to contradict the results of Kumar *et al.* [55] who reported Selenium vacancies in as-grown films. The apparent contradiction is explained by noting the different growth temperatures used in our work (room temperature) and Kumar *et al.* (425 °C). We observed Se rich films when grown at room temperature, whereas Kumar *et al.* report Se deficienct films when grown at 425 °C. Their data is consistent with our 350 °C vacuum-annealed sample which is significantly Se deficient (Table 1).

To conclude, we have compared our best data (250 °C annealed sample) with several reports available on 6-10 nm Bi_2Se_3 deposited on a variety of substrates in Table 3. At the ultrathin level, the literature is dominated by MBE films. Data from exfoliated Bi_2Se_3 is also included for comparison. Compared to the data on standard substrates such as Al_2O_3, Si, Si/SiO_2 at 300 K – and several reports at low temperatures – we note that our sputtered Bi_2Se_3 films grown on amorphous quartz have similar or lower carrier concentration and higher mobility values. On the other hand, there are several reports on MBE films with significantly lower carrier concentration and higher mobility values than our data[20,26,49,60,24]. In those reports, the films are grown either on lattice-matched or buffered substrates, and/or the authors employed high-field Hall measurements at low temperatures to extract the surface, bulk or impurity band mobilities using a multi-channel model. Such techniques are beyond the scope of this work. The reported surface mobility values are typically an order of magnitude higher than the bulk/impurity band mobilities, as indicated in Table 3. In our case, the Hall measurements are sensitive to bulk properties only. When bulk

Table 3
Reported carrier concentration and mobility values obtained by several groups on ultra-thin Bi_2Se_3 films. Abbreviations used: FET= Field-effect-transistor, HFH= High-field Hall, QWS=Quantum Well state, TS= Terahertz Spectroscopy.

Thickness (nm)	Growth Method	Subst.	n_{2D} (cm^{-2})	n_{3D} (cm^{-3})	μ (cm^2/V.s)	T (K)	Meas. Method
7	**This work**	**Quartz**	**1.07 × 10^{13}**	**1.34 × 10^{19}**	**112**	**300**	**Bulk, Hall**
20	Sputt. [35]	Si/SiO_2	-	(4-8) × 10^{20}	7-10	-	Bulk, Hall
9-54	Sputt. [36]	Al_2O_3	~ 10^{15}		0.26-8.8		Bulk, Hall
6	Sputt. [58]	Quartz	9.7 × 10^{13}	1.63 × 10^{20}	25	300	Bulk, Hall
6	PLD [32]	InP	1.3 × 10^{14}	-	10	-	Bulk, FET
6	PLD [34]	$SrTiO_3$	-	2.6 × 10^{19}	86	2	Bulk, FET
8	MBE [8]	Al_2O_3	9.4 × 10^{13}	-	-	300	Bulk, Hall
8	MBE [9]	Al_2O_3	3.8 × 10^{13}	-	-	300	Bulk, Hall
6	MBE [19]	Al_2O_3	3.5 × 10^{13}	-	350	2	Bulk, Hall
8	MBE [20]	Al_2O_3	~3 × 10^{13}	-	~500	2	Surface, HFH
8	MBE [20]	Al_2O_3	8 × 10^{12}	-	~3000	2	Surface, HFH
5	MBE [22]	SiO_2	-	~3 × 10^{20}	~5	300	Bulk, FET
10	MBE [24]	CdS	1.3 × 10^{13}	-	~380	2	Impurity, HFH
10	MBE [24]	CdS	0.04 × 10^{13}	-	~5000	2	Surface, HFH
10	MBE [26]	Al_2O_3	3.8 × 10^{13}	-	540	1.5	Bulk, HFH
10	MBE [26]	Al_2O_3	0.26 × 10^{13}	-	1550	-	Surface, HFH
7-8	MBE [48]	Si	~3.8 × 10^{13}	~5 × 10^{19}	~100-200	1.5	Bulk, HFH
5-50	MBE [49]	Sub[1]	(1-3) × 10^{12}	-	16,000	1.5	Surface, Hall
7	MBE [50]	SiO_2/Si	2.2 × 10^{13}	-	-	-	Bulk, FET
2-40	MBE [52]	Al_2O_3	-	(0.5-3.5) × 10^{19}	-	-	Bulk, Hall
8	MBE [60]	Si	8.4 × 10^{10}	-	2880	-	Surface, TS
8	MBE [60]	Si	4.5 × 10^{12}	-	54	-	QWS, TS
10	VWE [61]	Mica	~6.6 × 10^{13}	-	~100	300	Bulk, HFH
10	Exfoliated [62]	SiO_2/Si	~1 × 10^{13}	-	320 -1500	2	Bulk, FET

[1] $Al_2O_3/In_2Se_3/(Bi_{0.5}In_{0.8})_2Se_3$

properties are reported, our data compares very well with MBE work [48]. In our previous work, we have noted that ultra-thin films grown on Al_2O_3 substrates show higher mobility [58]. Taken together, we believe that the sputtered films will also show significant improvements if grown on lattice-matched substrates and such work will be undertaken in the future.

4. Conclusions

Transport properties of sub-10 nm Bi_2Se_3 thin-films fabricated using magnetron sputtering are investigated as a function of the post-deposition vacuum annealing temperature. As-deposited samples – grown at room temperature - – are Se-rich due to a disproportionately high rate of Selenium sputtering from the stoichiometric target. We observed the highest carrier concentration and mobility values when Se-rich samples are annealed at lower temperatures. The lowest carrier concentration ($\sim 1 \times 10^{19}$ cm^{-3}) and highest mobility (over 100 cm^2/V.s) are obtained in the 220-250 °C annealing temperature range. The crystal structure, on the other hand, is best at 300 °C when bismuth and selenium is in the stoichiometric 2:3 ratio. Overall, our work demonstrates that the transport properties of Bi_2Se_3 films are highly tunable through post-annealing temperature, which may be of interest in applied areas such as nanoelectronics and spintronics.

Declaration of Competing Interest

The authors declare that they have no known competing financial interests or personal relationships that could have appeared to influence the work reported in this paper.

Acknowledgements

The authors would like to acknowledge NSF CAREER grant (ECCS, Award # 1846829) for partial support of this work.

Credit Author Statement

The author names provided in the submission are correct and not changes to the authorship have been made.

References

[1] M.Z. Hassan, C.L. Kane, Colloquium: topological insulators, Rev. Mod. Phys. 82 (2010) 3045.
[2] J.E. Moore, The birth of topological insulators, Nature 464 (2010) 194–198.
[3] D. Hsieh, D. Qian, L. Wray, Y. Xia, Y.S. Hor, R.J. Cava, M.Z. Hasan, A topological Dirac insulator in a quantum spin Hall phase, Nature 452 (2008) 970–974.
[4] Y. Xia, D. Qian, D. Hsieh, L. Wray, A. Pal, H. Lin, A. Bansil, D. Grauer, Y.S. Hor, R. J. Cava, M.Z. Hasan, Observation of a large-gap topological insulator class with a single Dirac cone on the surface, Nat. Phys. 5 (2009) 398.
[5] D. Hsieh, Y. Xia, D. Qian, L. Wray, J.H. Dil, F. Meier, J. Osterwalder, L. Patthey, N. P. Checkelsky, A.V. Ong, H. Lin, A. Bansil, D. Grauer, Y.S. Hor, R.J. Cava, M. Z. Hasan, A tunable topological insulator in the spin helical Dirac transport regime, Nature 460 (2009) 1101.
[6] C.-F. Pai, Switching by topological insulators, Nat. Mater. 17 (2018) 755.
[7] M. DC, R. Grassi, J.-Y. Chen, M. Jamali, D.R. Hickey, D. Zhang, Z. Zhao, H. Li, P. Quarterman, Y. Lv, M. Li, A. Manchon, K.A. Mkhoyan, T. Low, J.-P. Wang, Room-temperature high spin-orbit torque due to quantum confinement in sputtered $Bi_xSe_{(1-x)}$ films, Nat. Mater. 17 (2018) 800.
[8] A.R. Mellnik, J.S. Lee, A. Richardella, J.L. Grab, P.J. Mintun, M.H. Fisher, A. Vaexi, A. Manchon, E.-A. Kim, N. Samarth, D.C. Ralph, Spin-transfer torque generated by a topological insulator, Nature 511 (2014) 449–451.
[9] Y. Wang, D. Zhu, Y. Yang, J. Yu, R. Ramaswamy, R. Mishra, S. Shi, M. Elyasi, K.-L. Teo, M. Elyasi, K.-L. Teo, Y. Wu, H. Yang, Room temperature magnetization switching in topological insulator-ferromagnetic heterostructure by spin-orbit torques, Nat. Commun. 8 (2017) 1364.
[10] N.H. Khang, Y. Ueda, P.N. Hai, A conductive topological insulator with large spin Hall effect for ultralow power spin-orbit torque switching, Nat. Mater. 17 (2018) 808.
[11] M.T. Philip, M.R. Hirsbrunner, M.J. Park, M.J. Gillbert, Performance of Topological Insulator Interconnects, IEEE Electron Device Lett 38 (2017) 138.
[12] P.D. Pietro, M. Ortolani, O. Limaj, A.D. Gaspare, V. Gioregianni, M. Brahlek, N. Bansal, N. Koirala, S. Oh, P. Calvani, S. Lupi, Observation of Dirac plasmons in a topologica insulator, Nat. Nanotechnol. 134 (2013).
[13] T. Ginley, Y. Wang, Z. Wang, S. Law, Dirac plasmons and beyond:the pas, present, and future of plasmonics in 3D topological insulators, MRS Commun. 1 (2018).
[14] X. Zhang, J. Wang, S.-C. Zhang, Topological insulators for high-perfomance terahertz to infrared applications, Phys. Rev. B 82 (2010).
[15] F. Giorgianni, E. Chiadroni, A. Rovere, M. Cestelli-Guidi, A. Perucchi, M. Bellaveglia, M. Castellano, D.D. Giovenale, G.D. Pirro, M. Ferrario, R. Pompili, C. Vaccarezza, F. Villa, A. Cianchi, A. Mostacci, M. Petrarca, M. Brahlek, N. Koirala, S. Oh, S. Lupi, Strong nonlinear terahertz response induced by Dirac surface states in Bi_2Se_3 topological insulator, Nat. Commun. 7 (2016) 11421.
[16] L. Fu, C.L. Kane, Superconducting proximity effect and Majorana fermions at the surface of a topological insulator, Phys. Rev. Lett. 100 (2008), 096407.
[17] A. Akhmerov, J. Nilsson, C. Beenakker, Electrically detected interferometry of Majorana fermions in a topological insulator, Phy. Rev. Lett. 102 (2009), 216404.
[18] G.J. Ferreira, D. Loss, Magnetically defined qubits on 3D topological insulators, Phys. Rev. Lett. 111 (2013), 106802.
[19] M. Liu, C.-Z. Chang, Z. Zhang, Y. Zhang, W. Ruan, K. He, L.-I. Wang, X. Chen, J.-F. Jia, S.-C. Zhang, Q.-K. Xue, X. Ma, Y. Wang, Electron interaction-driven insulating ground state in Bi_2Se_3 topological insulators in the two-dimensional limit, Phys. Rev. B 83 (2011), 165440.
[20] N. Bansal, Y.S. Kim, M. Brahlek, E. Edrey, S. Oh, Thickness independent transport channels in topological insulator Bi_2Se_3 thin films, Phys. Rev. Lett. 109 (2012), 116804.
[21] A. Richardella, D.M. Zhang, J.S. Lee, A. Koser, D.W. Rench, A.L. Yeats, B. B. Buckley, D. Awschalom, N. Samarth, Coherent heteroepitaxy of Bi_2Se_3 on GaAs (111)b, App. Phys. Lett. 97 (2010), 262104.
[22] J.H. Jeon, M. Song, H. Kim, W.-J. Jang, J.-Y. Park, S. Yoon, S.-J. Kahng, Quintuple layer Bi_2Se_3 thin films directly grown on insulating SiO_2 using molecular beam epitaxy, App. Surf. Sci. 316 (2014) 42–44.
[23] P. Tabor, C. Keenan, S. Urazhdin, D. Lederman, Molecular bean epitaxy and characterization of thin Bi_2Se_3 filmson Al_2O_3 (110), App. Phys. Lett. 99 (2011), 013111.
[24] L. He, F. Xiu, X. Yu, M. Teague, W. Jiang, Y. Fan, X. Kou, M. Lang, Y. Wang, G. Huang, N.-C. Yeh, K.L. Wang, Surface-dominated conduction in a 6 nm thick Bi_2Se_3 thin film, Nano Lett. 12 (2012) 1486–1490.
[25] S.-K. Jerng, K. Joo, Y. Kim, S.-M. Yoon, J.H. Lee, M. Kim, J.S. Kim, E. Yoon, S.-H. Chun, Y.S. Kim, Ordered growth of topological insulator Bi_2Se_3 thin films on dielectric amourphous SiO_2 by MBE, Nanoscale 5 (2013) 10618.
[26] A.A. Taskin, S. Sasaki, K. Segawa, Y. Ando, Manifestation of topological protection in transport properties of epitaxial Bi_2Se_3 thin films, Phys. Rev. Lett. 109 (2012), 066803.
[27] H.D. Li, Z.Y. Wang, X. Kan, X. Guo, H.T. He, Z. Wang, J.N. Wang, T.L. Wong, N. Wang, M.H. Xie, The van der Waals epitaxy of Bi_2Se_3 on the vicinal Si (111) surface: an approach for preparing high-quality thin films of a topological insulator, New J. Phys. 12 (2010), 103038.
[28] Y.-C. Lin, Y.-S. Chen, C.-C. Lee, J.-K. Wu, H.-Y. Lee, C.-T. Liang, Y.H. Chang, A study on the epitaxial Bi_2Se_3 thin film grown by vapor phase epitaxy, AIP Adv. 6 (2016), 065218.
[29] J.E. Brom, Y. Ke, R. Du, D. Won, X. Weng, K. Andre, J.C. Gagnon, S.E. Mohney, Q. Li, K. Chen, X.X. Xi, J.M. Redwing, Structural and electrical properties of epitaxial Bi_2Se_3 thin films grown by hybrid physical-chemical vapor deposition, App. Phys. Lett. 100 (2012), 162110.
[30] Z. Liao, M. Brahlek, J.M. Ok, L. Nuckols, Y. Sharma, Q. Lu, Y. Zhang, H.N. Lee, Pulsed-laser epitaxy of topological insulator Bi_2Te_3 thin films, APL Mater. 7 (2019), 041101.
[31] L. Meng, H. Meng, W. Gong, W. Liu, Z. Zhang, Growth and characterization of Bi_2Se_3 thin films by pulsed laser deposition using alloy target, Thin Solid Films 519 (2011) 7627–7631.
[32] Y. Onose, R. Yoshimi, A. Tsukazki, H. Yuan, T. Hidaka, Y. Iwasa, M. Kawasaki, Y. Tokura, Pulsed laser deposition and ionic liquid gate control of epitaxial Bi_2Se_3 thin films, App. Phys. Exp. 4 (2011), 083001.
[33] Y.F. Lee, R. Kumar, F. Hunte, J. Narayan, J. Schwartz, Microstructure and transport properties of epitaxial topological insulator Bi_2Se_3 thin films grown on MgO (100), Cr_2O_3 (0001), and Al_2O_3 (0001) templates, J. App. Phys. 118 (2015), 125309.
[34] L. Yang, Z. Wang, M. Li, X.P.A. Gao, Z. Zhang, The dimensional crossover of quantum transport properties in few-layered Bi_2Se_3 thin films, Nanoscale Adv. 1 (2019) 2303–2310.
[35] P. Sahu, J.-Y. Chen, J.C. Myers, J.-P. Wang, Weak Antilocalization and low-temperature characterization of sputtered polycrystalline bismuth selenide, App. Phys. Lett. 112 (2018), 122402.
[36] W.J. Wang, K.H. Gao, Q.L. Li, Z.-Q. Li, Disorder-dominated linear magnetoresistance in topological insulator Bi_2Se_3 thin films, App. Phys. Lett. 111 (2017), 232105.
[37] W.J. Wang, K.H. Gao, Z.Q. Li, Thickness-dependent transport channels in topological insulator Bi_2Se_3 thin films grown by magnetron sputtering, Sci. Rep. 6 (2016) 25291.
[38] T.P. Ginley, Y. Wang, S. Law, Topological insulator film growth by molecular beam epitaxy: a review, Crystals 6 (2016) 154.
[39] Y. Guo, Z. Liu, H. Peng, A roadmap for controlled production of topological insulator nanostructures and thin films, Small 11 (2015) 3290–3305.
[40] L. He, X. Kou, L.K. Wang, Review of 3D topological insulator thin-film growth by molecular beam epitaxy and potential applications, Phys. Status Solidi RRL 7 (2013) 6218–6254.

[41] W. Tian, W. Yu, J. Shi, Y. Wang, The property, preparation and application of topological insulators: a review, Materials 10 (2017) 814.
[42] P.O. Oviroh, R. Akbarzadeh, D. Pan, R.A.M. Coetzee, T.-C. Jen, New development of atomic layer deposition: process, methods and applications, Sci. Technol. Adv. Mater. 20 (2019) 465–496.
[43] L. Xue, P. Zhou, C.X. Zhang, C.Y. He, G.L. Hao, L.Z. Sun, J.X. Zhong, First-principles study of native point defects in Bi_2Se_3, AIP Adv. 3 (2013), 052105.
[44] S. Urazhdin, D. Bilc, S.H. Tessmer, S.D. Mahanti, T. Kyratsi, M.G. Kanatzidis, Scanning tunneling microscopy of defect states in the semiconductor Bi_2Se_3, Phys. Rev. B 66 (2002), 161306.
[45] J.G. Analytis, J.-H. Chu, Y. Chen, F. Corredor, R.D. McDonald, Z.X. Shen, I. R. Fisher, Bulk Fermi surface coexistence with Dirac surface state in Bi_2Se_3: A comparison of photoemission and Shubnikov-de Haas measurements, Phys. Rev. B. 81 (2010), 205407.
[46] C.-L. Song, Y.-L. Wang, Y.-P. Jiang, Y. Zhang, C.-Z. Chang, L. Wang, K. He, X. Chen, J.-F. Jia, Y. Wang, Z. Fang, X. Dai, X.-C. Xie, X.-L. Qi, S.-C. Zhang, Q.-K. Xue, X. Ma, Topological insulator Bi_2Se_3 thin films grown on double-layer graphene by molecular beam epitaxy, Appl. Phys. Lett. 97 (2010), 143118.
[47] N.P. Butch, K. Kirshenbaum, P. Syers, A.B. Sushkov, G.S. Jenkins, H.D. Drew, J. Paglione, Strong surface scattering in ultrahigh-mobility Bi_2Se_3 topological insulator crystals, Phys. Rev. B 81 (2010), 241301.
[48] Y.S. Kim, M. Brahlek, N. Bansal, E. Edrey, G.A. Kapilevich, K. Lida, M. Tanimura, Y. Horibe, S.-W. Cheong, S. Oh, Thickness-dependent bulk properties and weak antilocalization effect in topological insulator Bi_2Se_3, Phys. Rev. B 84 (2011), 073109.
[49] N. Koirala, S. Brahlek, M. Salehi, L. Wu, J. Dai, J. Waugh, T. Nummy, M.-G. Han, J. Moon, Y. Zhu, D. Dessau, W. Wu, N.P. Armitage, S. Oh, Record surface state mobility and quantum hall effect in topological insulator thin films via interface engineering, Nano Lett. 15 (2015) 8245–8249.
[50] Y.H. Liu, C.W. Chong, J.L. Jheng, S.Y. Huang, J.C.A. Huang, Z. Li, H. Qiu, S. H. Huang, V.V. Marchenkov, Gate-tunable coherent transport in Se-capped Bi_2Se_3 grown on amourphous SiO_2/Si, Appl. Phys. Lett. 107 (2015), 012106.
[51] L. He, F. Xiu, Y. Wang, A.V. Fedorov, G. Huang, X. Kou, M. Lang, W.P. Beyermann, J. Zou, K.L. Wang, Epitaxial growth of Bi_2Se_3 topological insulator thin films on Si (111), J. Appl. Phys. 109 (2011), 103702.
[52] Y.D. Glinka, S. Babakiray, D. Lederman, Plasmon-enhanced electron-phonon coupling in Dirac surface states of the thin-film topological insulator Bi_2Se_3, J. Appl. Phys. 118 (2015), 135713.
[53] C. Zhang, X. Yuan, K. Wang, Z.-G. Chen, B. Cao, W. Wang, Y. Liu, J. Zou, F. Xiu, Observation of a metal-insulator transition and strong surface states in $Bi_{2-x}Sb_xSe_3$ thin films, Adv. Mater. 26 (2014) 7110–7115.
[54] Z.T. Wei, M. Zhang, Y. Yan, X. Kan, Z. Yu, Y.L. Chen, X.S. Yang, Y. Zhao, Transport properties of Bi_2Se_3 thin films grown by magnetron sputtering, Funct. Mater. Lett. 2015 (2015), 1550020.
[55] R. Kumar, A.K. Yadav, A. Biswas, M. Nand, J. Bahadur, S. Ghosh, S.N. Jha, D. Bhattacharyya, Crystalline Bi_2Se_3 topological insulator films prepared by dc magnetron sputtering, Vacuum 177 (2020), 109366.
[56] M. Zhang, Z. Wei, R. Jin, Y. Ji, Y. Yan, X. Pu, X. Yang, Y. Zhao, Electrical transport properties and morphology of topological insulator Bi_2Se_3 thin films with different thickness prepared by magnetron sputtering, Thin Solid Films 603 (2016) 289–293.
[57] Y.R. Sapkota, A. Alkabash, A. Walber, H. Samassekou, D. Mazumdar, Optical evidence for blue shift in topological insulator bismuth selenide in the few-layer limit, Appl. Phys. Lett. 110 (2017) 18190.
[58] Y.R. Sapkota, D. Mazumdar, Bulk transport properties of bismuth selenide thin films grown by magnetron sputtering approaching the two-dimensional limit, J. Appl. Phys. 124 (2018), 105306.
[59] D. Kim, Q. Li, P. Syers, N.P. Butch, J. Paglione, S.D. Sarma, M.S. Fuhrer, Intrinsic electron-phonon resistivity of Bi_2Se_3 in the topological regime, Phys. Rev. Lett. 109 (2012), 166801.
[60] B.C. Park, T.-H. Kim, K.I. Sim, B. Kang, J.W. Kim, B. Cho, K.-H. Jeong, M.-H. Cho, J. H. Kim, Terahertz single conductance quantum and topological phase transitions in topological insulator Bi_2Se_3 ultrathin films, Nat. Commun. 6 (2015) 6552.
[61] Y. Jing, S. Huang, K. Zhang, J. Wu, Y. Guo, H. Peng, Z. Liu, H.Q. Xu, Weak antilocalization and electron-electron interaction in coupled multiple-channel transport in a Bi_2Se_3 thin film, Nanoscale 8 (2016) 1879–1885.
[62] D. Kim, S. Cho, N.P. Butch, P. Syers, K. Kirshenbaum, S. Adam, J. Paglione, M. S. Fuhrer, Surface conduction of topological Dirac electrons in bulk insulating Bi_2Se_3, Nat. Phys. 8 (2012) 459–463.